atoms

MDPI

Article

Study of the Triplet States in the Autoionizing Electron Spectra of He and Ar Induced by Low-Energy Electrons

Bratislav P. Marinković [1,*], Lorenzo Avaldi [2] and Jozo J. Jureta [1]

[1] Laboratory for Atomic Collision Processes, Institute of Physics Belgrade, University of Belgrade, Pregrevica 118, 11080 Belgrade, Serbia; jureta@ipb.ac.rs
[2] CNR-Istituto di Struttura della Materia, Area della Ricerca di Roma 1, CP10, 00015 Monterotondo Scalo, Italy; lorenzo.avaldi@ism.cnr.it
* Correspondence: bratislav.marinkovic@ipb.ac.rs; Tel.: +381-11-316-0882

Abstract

In this work, the He and Ar triplet autoionizing states have been studied using a non-monochromatic electron beam and a high-resolution electrostatic analyzer at low incident electron energies and three ejection angles: 40°, 90°, and 130°. Low-energy electrons have been used because they have a high probability of exciting triplet states regardless of whether they are discrete isolate states or are embedded in the ionization continuum. Additionally, the He ejected electron spectra have been measured at several ejection angles between 20° and 130° and two incident energies, namely 60.5 eV and 101 eV. The anisotropic angular distributions indicate that orbital angular momentum exchange between the ejected and scattered electrons occurred. The energies of the first triplets $3s3p^6 4s(^3S)$ and $3s3p^6 4p(^3P)$ states of argon are found to be (24.985 ± 0.020) eV and (26.52 ± 0.02) eV, respectively.

Keywords: triplet states; autoionization; helium; argon; ejected electron spectroscopy

1. Introduction

He and Ar autoionization states excited by low-energy electron impact have not been studied systemically in the past in comparison, for example, to the extensive studies in the Auger energy region [1,2]. This is due to the very low signal-to-background ratio for these states embedded in the continuum and the insufficient experimental resolution of the available setups. However, the low-energy region is very interesting because triplet states appear to be more intense compared to the corresponding ones observed at high impact energies. These measurements need not only high resolution in the electron analyzer, but also an experimental technique able to distinguish between ejected and scattered electrons when the incident energy is close to the threshold energy of an excited state [3]. Ejected electron spectra for rare gas atoms in the threshold region are reported in [4], and for helium in [5–9] and argon in [10–14].

Spectra obtained at low impact energies are often affected by post-collision interaction (PCI), which manifests as energy shift and asymmetric line shape in the peaks of certain excited states within the auto-ionization region, particularly as the incident energy approaches the excitation threshold. This phenomenon has been qualitatively explained [6,7] as the exchange energy and momentum between the two free electrons, the ejected and scattered ones, produced in the vicinity of the threshold of a short-lived excited state in the Coulomb field of the ion. High-precision calculations have been recently performed

Academic Editor: Jean-Christophe Pain

Received: 3 January 2026
Revised: 27 January 2026
Accepted: 30 January 2026
Published: 31 January 2026

for near-threshold excitation of the $(1s3s)^{3,1}S$ states of He, which are influenced by many resonances [15].

Most experimental studies on the electron-induced excitation of autoionizing states on rare gases were conducted nearly 50 years ago. Their results provide a valuable body of information, which, however, is sparse in several papers; each of them often contains information limited to a small region of incident and/or ejected energies. Moreover, different experimental procedures have been adopted, some of them affected by the technological limits of that time. We have undertaken a systematic investigation of the ejected electron spectra of rare gases using the same setup and procedures.

The present work continues our previous measurements of ejected electron spectra of He [16] and Ar [17] performed at higher electron incident energies. Here, we investigate the low incident electron energies, using impact energies below the double ionization of both He (79.004 eV) and Ar (43.39 eV). In the case of the study of the angular dependence in He, a higher energy (101 eV) has been used to overlap with our previous measurements [17]. In He, we have studied two autoionizingstates, the $(2s^2)^1S$ and $(2s2p)^3P$, in the low incident energy region from 58.5 eV to 70.6 eV. This energy region corresponds roughly to 2–10 eV above the threshold of the $(2s^2)^1S$ state at 57.8 eV. The objective of the Ar study is to determine the energies of the triplet states and to investigate variations in the shape and energy position of the $4s(^{3,1}S)$ states at small excess energy. Here, the excess energy is defined as the difference between the incident energy and the excitation energy of the state. In the low-energy region, all Ar autoionizingstates result from the excitation of the 3s electron to the ns, np, and nd subshells below the 3s ionization threshold at 29.24 eV, which corresponds to an ejected energy of 13.48 eV [18].

In the present study, we have remeasured the dependence of the $(2s^2)^1S$ autoionizationstates as a function of excess energy above their excitation energy. While the present measurements show substantial agreement with the spectra reported in [6], the observed behavior of the energy shift is predicted by the law later derived in [7]. A key result of the present study is the precise determination of the triplet autoionizing $4s(^3S)$ and $4p(^3P)$ in Ar.

2. Experimental Procedures and Methods

Details about the experimental setup can be found in refs. [16,17]. In the present experiment, a non-monochromatic electron beam operated in the energy region (27.7–101 $\pm$ 0.4 eV) collides with an effusive atomic beam let in the chamber via a platinum-iridium non-biased needle (0.5 mm diameter) in the perpendicular direction to the scattering plane. The interaction region has a cylindrical shape (ID 50 mm) made by the two cylinders of thin μ-metal foils with a separation of 10 mm in the collision plane in order to avoid the collection of scattered electrons from metal surfaces.

The ejected electrons after passing through a high-resolution hemispherical analyzer with a mean radius of 125 mm are detected by seven channeltrons. The spectra in these measurements are obtained in two modes of operation of the analyzer: the Constant Analyzer Energy (CAE) and the Constant Retarding Ratio (CRR) mode. This is carried out in order to compare their influence on the shape of the measured spectra at different excess energies. In the CAE mode, the analyzer pass energy is constant, while the kinetic energy is scanned by varying the retarding ratio of the lens stack. In this way, the energy resolution is constant. In the CRR mode, the ratio (K) between the kinetic energy (E_k) and the analyzer pass energy (E_p) during the scan is constant ($K \approx E_k/E_p$). CAE keeps the pass energy constant in the analyzer (i.e., energy resolution), but varies the behavior of the entrance lens. This may lead to a different solid angle accepted, i.e., either a large region of the interaction region is transported to the hemispheres or scattered electrons can be captured. CRR keeps the lens fixed and varies the pass energy. In this way, the solid angle

accepted is always the same, and the contribution of scattered electrons is the same at all energies. Of course, the resolution will change, but in the ejected energy investigated, this change is not relevant.

The background pressure in the vacuum chamber was 6×10^{-8} mbar, while the working pressure with gas in was 2×10^{-6} mbar. The accumulation time was 30 min for most of the spectra with an energy step of 0.020 eV per channel. The best resolution, defined as the full width at half maximum (FWHM) of the 3d(^{1}D) peak of Ar, was (0.040 ± 0.020) eV. The energy resolution of the He ejected electron spectra is determined by the combined effects of the analyzer energy resolution and the Doppler broadening, which is approximately 0.037 eV at a temperature of 350 K and a mean kinetic energy of 30 eV. The overall energy resolution was measured to be 0.060 eV FWHM). The transmission was not uniform, and all spectra are presented with subtracted background without any further normalization of the obtained spectra.

For calibration of the kinetic energy, the energy position of the He doubly excited 2s2p(^{1}P) state at 60.130 eV [19] has been used, while in Ar, the kinetic energies of the 3s3p^{6}4p(^{1}P) and 3s3p^{6}3d(^{1}D) states at 10.76 eV and 11.72 eV, respectively, have been used. The incident electron energy, E_e, scale was calibrated using the elastic channel with roughly 0.80 eV FWHM.

3. Results and Discussion

3.1. Helium

3.1.1. Energy Dependence of the 2s^2(^{1}S) and 2s2p(^{3}P) States

Figures 1a,b–3a,b show a series of He auto-ionizing spectra obtained in the CAE and CRR modes at ejection angles of 40°, 90°, 130°, respectively, and various incident energies. The ^{1}S peak shifts towards higher ejected energy when the incident energy reduces, while the ^{3}P peak does not show any change in energy position. The ^{3}P peak is definitely more intense at the ejection angles of 40° and 130°, while at 90°, both peaks have approximately the same intensity.

In Figure 1a,b changes in two spectra at incident energies 62.6 and 61.5 eV (i.e., at 4.8 and 3.7 eV) are visible. We observe an energy shift of the 2s^2(^{1}S) state due to PCI and a variation of the line shape of the peak due to the 2s2p(^{3}P) state as a consequence of the interference between the ejected and scattered electrons. This behavior has also been noticed in [20] but at smaller excess energies, i.e., 2.08 and 2.31 eV above the ionization energy of the 2s^2(^{1}S) state. At 60.5 eV (2.7 eV excess energy), the PCI shift is still visible, while at 59.5 eV (1.7 eV excess energy), in Figure 1a, the signal of the 2s^2(^{1}S) state either vanishes or overlaps with the tiny one of the 2s2p(^{3}P) state. The spectra at 61.5 eV in the CAE mode (Figure 1a) and 59.5 eV in the CRR mode (Figure 1b) display a similar shape to the spectra at 60.2 eV obtained in constant energy-loss mode in [6].

Differences in the shapes and intensities of the peaks exist between the spectra measured at 90° and 40° ejection angles. The four spectra in Figure 2a obtained between 68.6 and 62.6 eV incident energies show a weak influence of the PCI effect, but a broadening of the line shape due to the decay via a nearby negative ion resonance [1]. In the following two spectra at 61.5 and 60.5 eV incident energy, the PCI effect is visible as a shift of the ^{1}S state. A minor influence of the interference effect, which may be present between 60.5 and 61.5 eV (2.7 and 3.7 eV excess energies), is observed. As the incident energy decreases, the feature due to the ^{1}S state approaches that of the ^{3}P state, and at the lowest energy, the two structures overlap, hampering the definition of the change in the line shape due to the interference effect. In the CRR mode (Figure 2b), the spectra are characterized by better statistics than in the CAE mode. At 62.6 and 61.6 eV, the spectra show a small shift and some broadening of the line shape, while at 60.5 and 59.5 eV, they show larger shifts and

broadenings of the ^{1}S state and large changes in the line shape due to interference effects in the ^{3}P state. A comparison of the spectrum at 60.5 eV in the CRR mode with the spectrum in [6] at 95° shows a good agreement.

The spectrum at 68.6 eV obtained in the CAE mode (Figure 3a) has a different shape in the region of the ^{3}P state than the spectrum at 70.6 eV (Figure 3b) in the CRR mode, although the energy difference is only 2 eV. The spectrum at 65.6 eV in CRR mode shows the same shape as the spectrum at 66.6 eV in the CAE mode. The two spectra at 60.5 and 59.5 eV (Figure 3b) show a visible influence of the PCI and interference effects, indicating that, as in the measurements at 40° ejection angles (Figure 1b), these effects persist in the excess energy region 1.7 to 2.7 eV.

A comparison between the spectrum at 60.5 eV shown in Figure 3b and the spectrum at 115° and 60.2 eV reported in [6] indicates that our results obtained in the CRR mode are very similar in form to those obtained in the constant energy-loss mode.

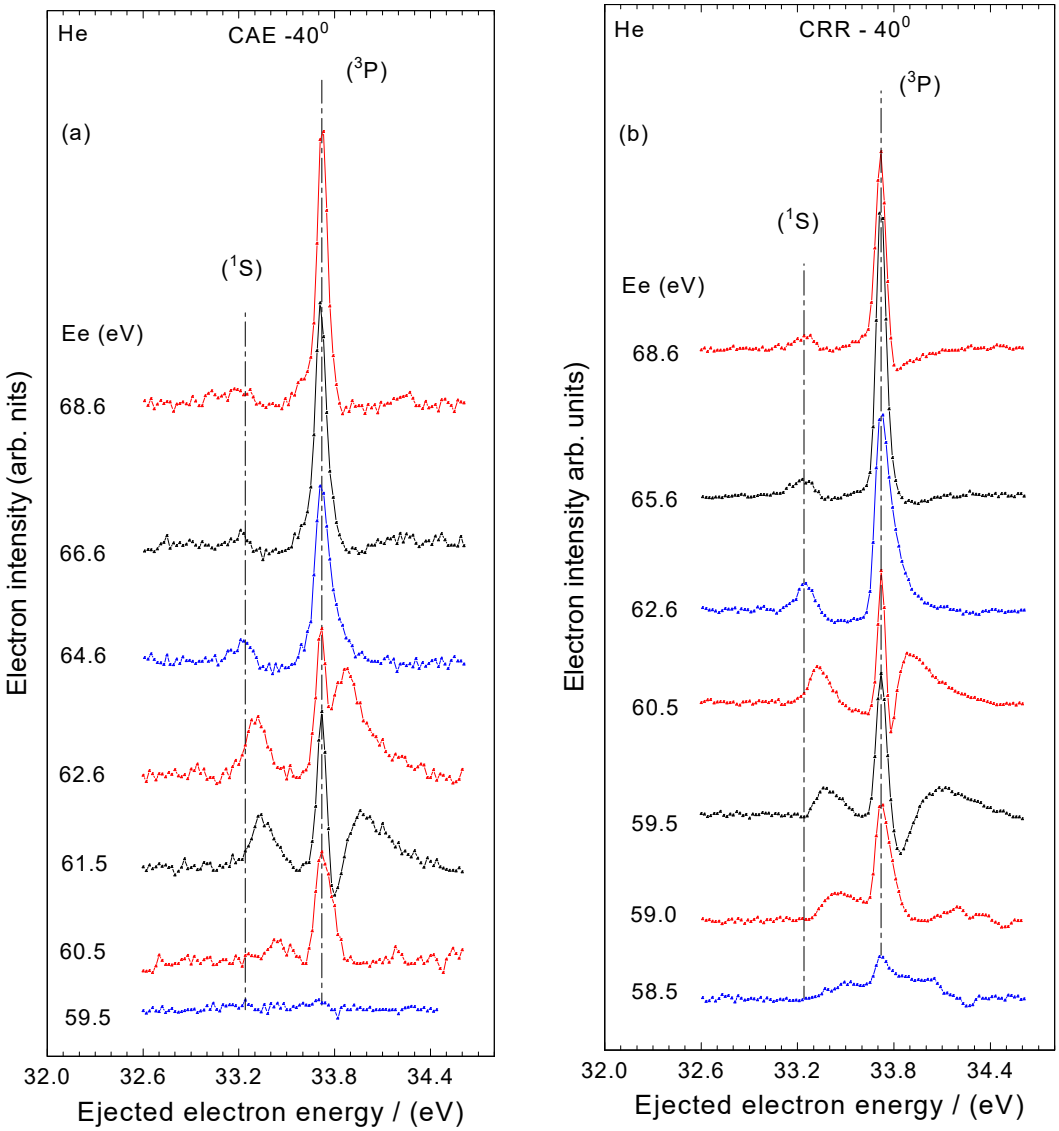

Figure 1. Ejected electron spectra of the first two He excited states measured at 40° ejection angle: (**a**) in the CAE mode; (**b**) in the CRR mode. Each spectrum is presented with a linear background subtracted and is obtained at constant incident electron energy (58.5–68.6) eV as indicated on the left-hand side. The ejected energy region between 32.6 and 34.6 eV was scanned with an energy step of 0.020 eV. Long dashed lines represent the energies of the $(2s^2)^1$S (57.8 eV excitation energy) and $(2s2p)^3$P (58.3 eV excitation energy) states.

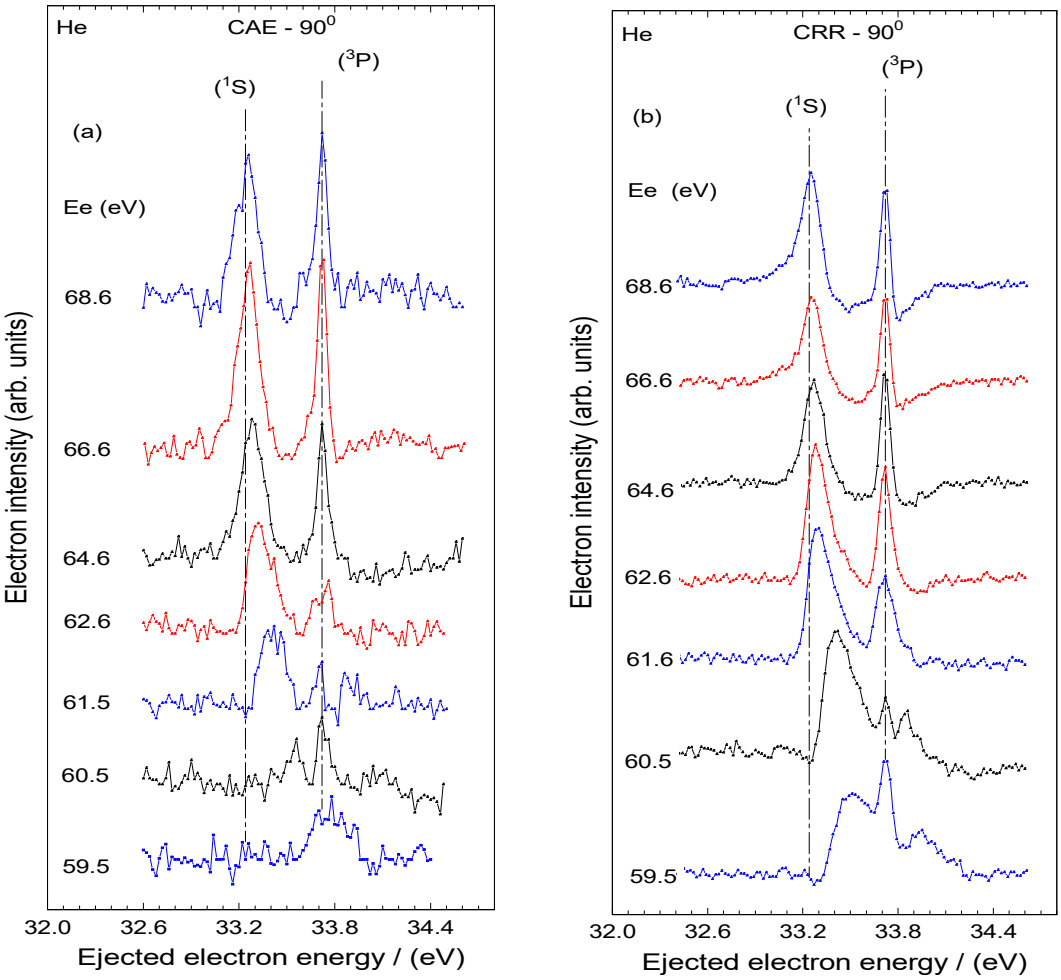

Figure 2. Ejected electron spectra of the first two He excited states measured at 90° ejection angle: (**a**) in the CAE mode; (**b**) in the CRR mode. Each spectrum is presented with a linear background subtracted and is obtained at constant incident electron energy (59.5–68.6) eV as indicated on the left-hand side. The ejected energy region between 32.6 and 34.6 eV was scanned with an energy step of 0.020 eV. Long dashed lines represent the energies of the $(2s^2)^1S$ (57.8 eV excitation energy) and $(2s2p)^3P$ (58.3 eV excitation energy) states.

3.1.2. Angular Dependence of the $2s^2(^1S)$ and $2s2p(^3P)$ States

Figure 4 shows the angular dependence of the $(2s^2)^1S$ and $(2s2p)^3P$ states at two constant incident energies of 60.5 eV and 101 eV obtained in the CRR mode. These two series of spectra are chosen to show the influence of the PCI effect on the shape and energy positions of the $2s^2(^1S)$ state at excess energies of 2.7 eV (Figure 4a) and 43.2 eV (Figure 4b).

The series of spectra at 60.5 eV shows the influence of the PCI and changes in the line shape. In the spectrum at an ejection angle of 20°, the $2s^2(^1S)$ state is seen with low intensity. In comparison with the spectrum at 22° in [6], one can notice large differences in the shape of the spectra between the two measurements. The observed differences in the spectra are attributed to the two distinct collection modes. In the present work, both ejected and inelastically scattered electrons are measured, whereas in [6] the constant energy-loss mode was employed, in which only ejected electrons were collected. The spectra at all other angles look very similar in the present measurement and in [6]. Present spectra between 30° and 130° show the influence of the PCI effect together with variation of the line shape of the ^3P state, especially pronounced between 50° and 115°.

The series of spectra at 101 eV (Figure 4b) shows completely different shapes of the $(2s^2)^1S$ state at all ejection angles in comparison with spectra at 60.5 eV. The spectra show typical Beutler–Fano line shapes depending on ejection angles. At 70° ejection angle, the $(2s^2)^1S$ state appears as a window resonance with an almost symmetric shape. Its width of 0.160 ± 0.020 eV is the same as that of the peak at130°.

These two series of spectra show an anisotropic angular distribution that indicates that an orbital angular momentum exchange between the two electrons, the ejected and inelastically scattered ones, occurs in both the energy region affected by PCI and outside it [21]. The angular distributions of ejected electrons from the $(2s^2)^1S$ state were measured by van der Burgt et al. [22] in the energy region from 0 to 0.5 eV above the threshold. They concluded that the direct excitation of this state starts 0.5 eV above the threshold. In the present work, our results show that already at 1.7 ± 0.4 eV excess energy in the CAE mode, the direct excitation dominates the production of ejected electrons. A comparison between spectra at 100 eV in [5] with present spectra at 30° and 130° in the CRR mode (Figure 4b) shows good agreement in the shape of the spectra, with the present experimental data showing better resolution.

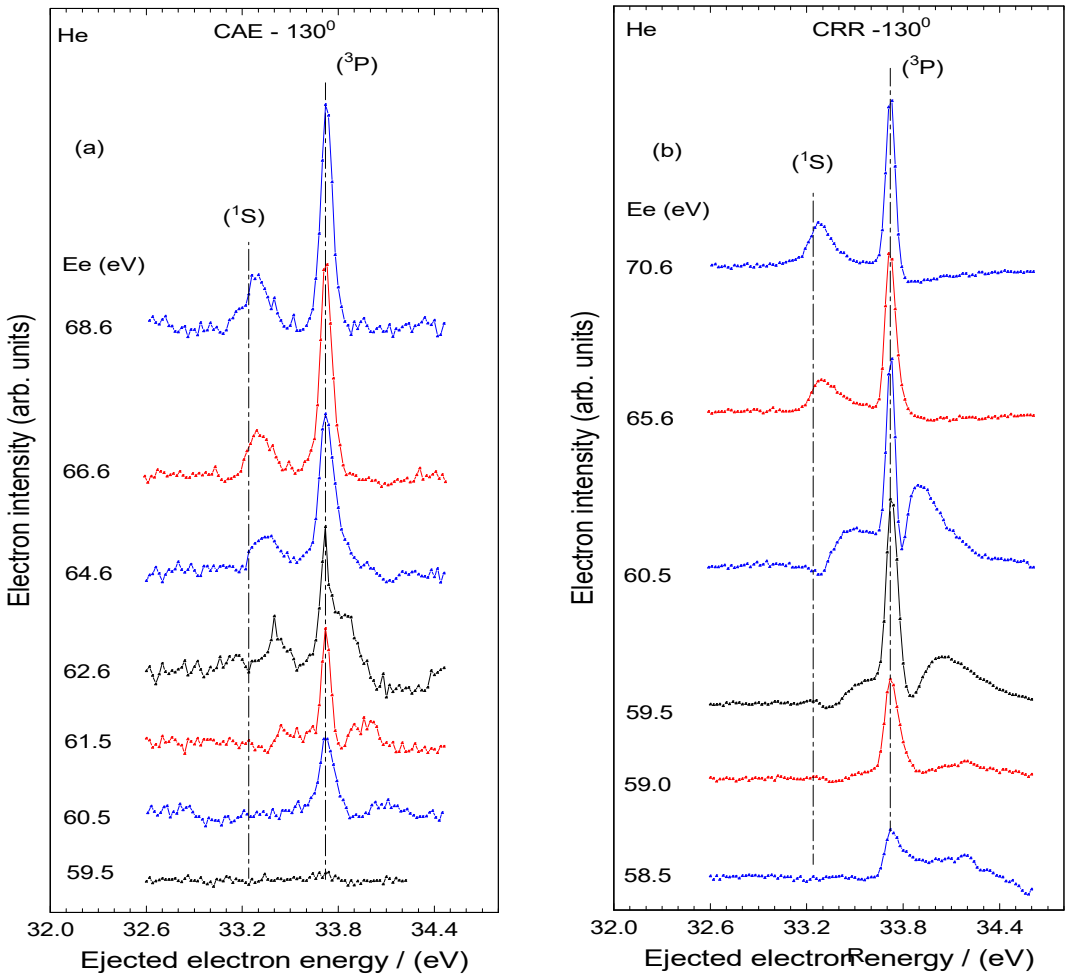

Figure 3. Ejected electron spectra of the first two He excited states measured at 130° ejection angle: (**a**) in the CAE mode; (**b**) in the CRR mode. Each spectrum is presented with a linear background subtracted and is obtained at constant incident electron energy (58.5–68.6) eV as indicated on the left-hand side. The ejected energy region between 32.6 and 34.6 eV was scanned with an energy step of 0.020 eV. Long dashed lines represent the energies of the $(2s^2)^1S$ (57.8 eV excitation energy) and $(2s2p)^3P$ (58.3 eV excitation energy) states.

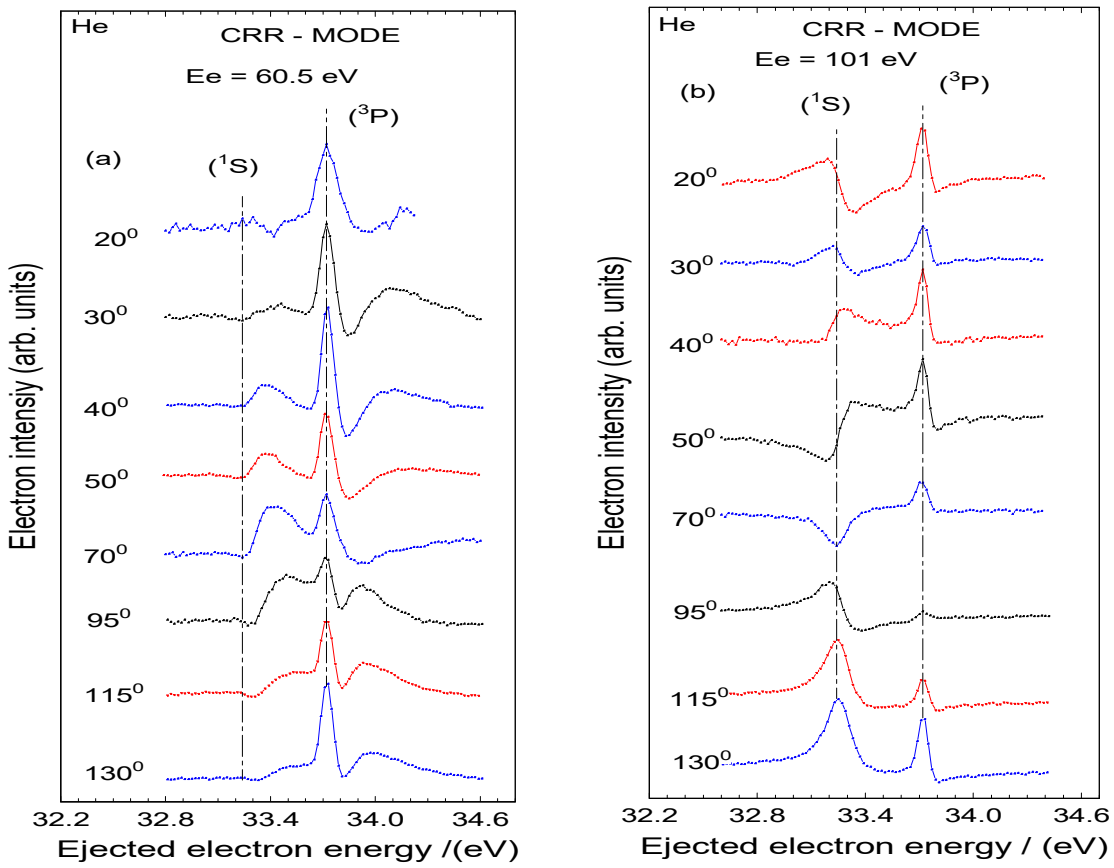

Figure 4. Angular dependence of the $2s^2(^1S)$ and $2s2sp(^3P)$ states in the CRR mode at constant electron incident energies of: (**a**) 60.5 eV; (**b**) 101 eV. The spectra (**a**) correspond to the excess energy of 2.7 eV above the threshold of the (^1S) state at 57.8 eV, while the spectra (**b**) correspond to the excess energy of 43.2 eV. The ejected energy region between 32.4 and 34.6 eV was scanned with energy steps of 0.020 eV.

3.1.3. Intensity Ratio of the $2s^2(^1S)$ and $2s2p(^3P)$ States

Figure 5 shows the intensity ratio between the $(2s^2)^1S$ and $(2s2p)^3P$ states in the CAE mode. Figure 5a shows the intensity ratio as a function of the incident energies (64.6, 66.6, and 68.6 eV) at three ejection angles, 40°, 90°, and 130°, while Figure 5b shows the intensity ratio as a function of ejection angles (40°, 90°, and 130°) at three incident energies, 64.6, 66.6, and 68.6 eV. These three energies have been chosen because the shapes of the peaks are not influenced by the PCI effect. In Figure 5a, the ratio exhibits a linear dependence on the incident energy, whereas in Figure 5b, the ratios of peaks at 90° indicate that the $(2s^2)^1S$ state has a very low intensity compared with the $(2s2p)^3P$ state at small and large ejection angles.

The smallest linewidth, measured as FWHM, of the $(2s^2)^1S$ is (0.120 ± 0.020) eV in the CRR mode and (0.140 ± 0.020) eV in CAE mode. These values are in good agreement with the value of 0.138 eV obtained in [6]. The smallest linewidth of the $(2s2p)^3P$ state is found to be (0.060 ± 0.020) eV independent of the mode of operation or ejected angle.

3.1.4. The PCI Effect on the $(2s^2)^1S$ State

Figure 6 shows the energy shift of the $(2s^2)^1S$ state due to the influence of the PCI effect in the CAE and CRR modes, taken from Figure 2, where the $(2s^2)^1S$ state appears as a peak. The energy shift, $E_{sh.}$, as a function of excess energy, is represented by the equation $E_{sh.} \propto \Delta E^{\beta}$, where the coefficient β is the free parameter in the fit [23].

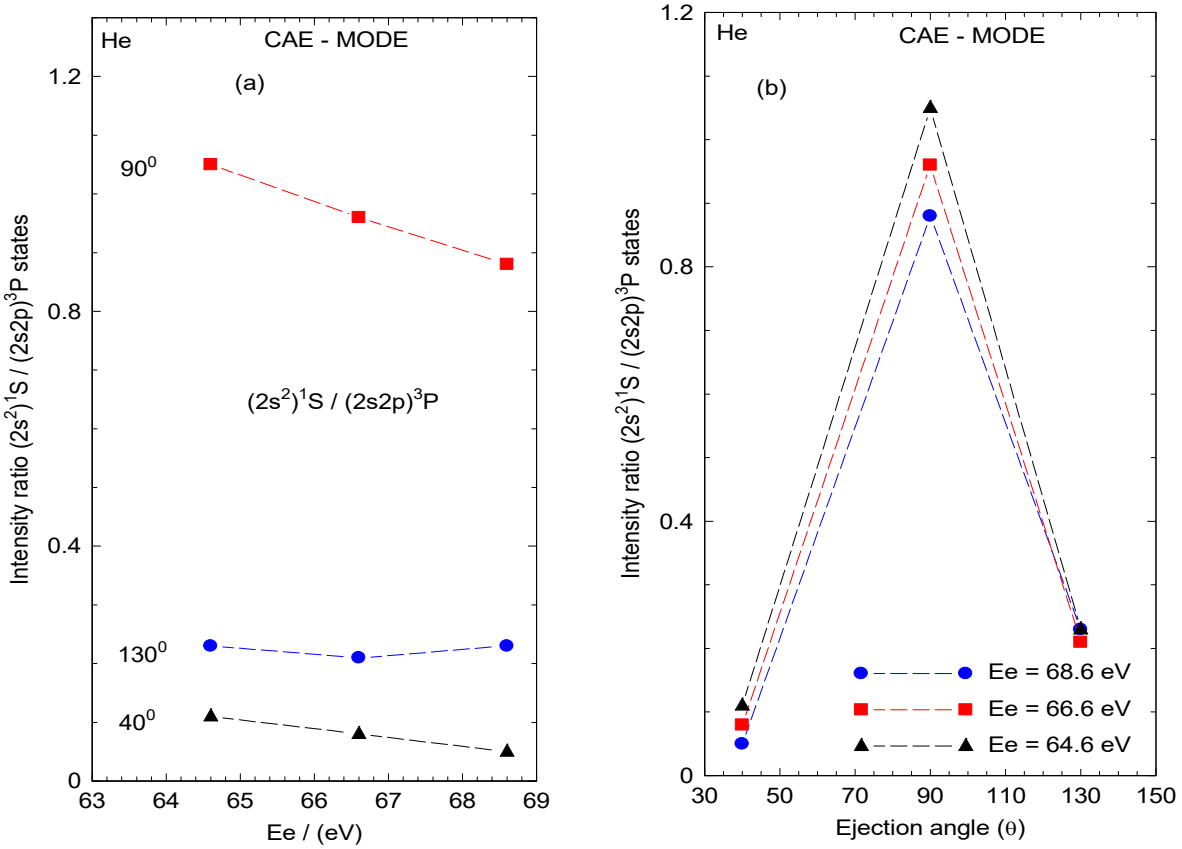

Figure 5. The intensity ratio of the $(2s^2)^1S$ and $(2s2p)^3P$ states obtained in the CAE mode as a function of: (**a**) incident electron energy Ee (eV) at three ejection angles 40°, 90°, and 130°; (**b**) ejection angle at three incident energies 64.6, 66.6, and 68.6 eV. Dashed lines between points serve to guide the eye.

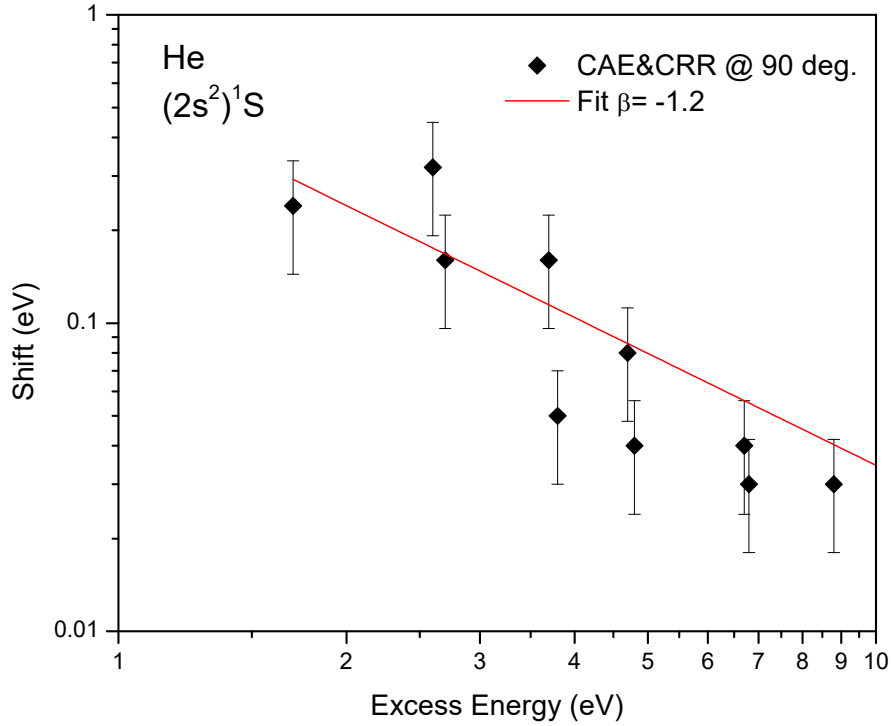

Figure 6. The log-log plot of the energy shift (eV) of the $(2s^2)^1S$ state due to the PCI effect measured in both the CRR and CAE modes at ejection angle 90°. The best fit of the combined data (CAE and CRR) results in an exponent of $\beta = -1.2 \pm 0.2$.

The best fit of present data gives an exponent of $\beta = -1.2 \pm 0.2$ in good agreement with the measurements of Smith et al. [7] and Spence [9]. The coefficient β is the free parameter, which, according to Smith et al. [7], should account for the energy of the inelastically scattered electron, the lifetime of the autoionizing state, and likely other parameters such as its polarizability. They suggested that the difference between this value and the 0.5 found previously in ion collisions may be due to a shorter lifetime of the autoionizingstates due to the presence of a scattered electron in the vicinity of the excited state.

3.2. Argon

Argon has a more complex electronic structure than He, resulting in a richer spectrum of auto-ionizing states. Consequently, the study of argon may be regarded as an extension of methodologies previously validated for helium. In the present work, we restrict our investigation to electron impact energies below the Ar^{2+} ionization threshold, to achieve experimental conditions comparable to those of the helium case.

Figures 7–9 show the series of Ar autoionizingspectra in the ejected energy region 8.5–13.6 eV measured at 40°, 90°, and 130° ejection angles and electron incident energy between 27 and 41 eV in both CAE and CRR operation modes of the analyzer. Figures show a large number of discrete features superimposed on a background whose shape depends on the incident electron energy and ejection angles. All features result from the single excitation of the 3s electron to the ns, np ($n \geq 4$), and nd ($n \geq 3$) states. Their energies and assignments, determined from the discussion in the following section, are presented in Table 1. The energy values are derived from spectra at 40°, where the line shapes of the peaks are mainly symmetric. The main characteristic of the spectra is the appearance of the most intense features in the form of doublets with an energy separation of 0.18 eV, which corresponds to the spin-orbit splitting of the ion core. The doublets are seen in other ejected spectra with both high [11,14,24] and low resolution [25].

3.2.1. The 4s(^{3,1}S) States

The peaks observed at the lowest energies of the spectra in Figures 7–9 belong to the 4s(^{3,1}S) states and are labeled as 1–1′ and 2–2′. Here we have two excited states, namely the ^{3}S and ^{1}S ones, and two final states Ar^+ ($3p_{3/2,1/2}{}^{-1}$), thus we observe four features. The peaks 1 and 2 are well defined with FWHM of approximately 90 meV and energy separation of 0.18 eV, while the third feature 1′ has an asymmetric shape (FWHM ~230 meV) depending on incident energy and ejection angle. The feature 2′ has low intensity. A similar intensity distribution has been noticed earlier [14].

To find the energy positions of the 4s(^{3,1}S) states obtained in the present experiment at low incident electron energies, we make an analysis of the spectrum at an incident energy of 41.22 eV and three ejection angles shown in Figure 10. The spectra show two doublets, (1–1′) and (2–2′), indicated by long dashed lines. The peaks (1, 2) are well defined and not sensitive to ejection angles, while the peaks (1′, 2′) are very sensitive to ejection angles, probably due to the variation of the underlying spectrum of scattered electrons. The energy separations between peaks (1, 2) and (1′, 2′) are 0.17 and 0.16 eV, respectively, while the ones between peaks (1, 1′) and (2, 2′) are 0.31 and 0.30 eV, respectively. Energies of the first doublet are 24.99 eV (9.05 + 15.94) and 25.30 eV (9.36 + 15.94). Energies of the second doublet are 24.98 eV (9.22 + 15.76) and 25.28 eV (9.52 + 15.76). The lower energy 24.985 eV (mean value) is attributed to the 4s(^{3}S) state, and the energy 25.29 eV (mean value) is attributed to the 4s(^{1}S) state. A comparison with other references reported in Table 1 shows good agreement with all others for the triplet state. For the singlet state, good agreement is found with [10,11,26,27], but some discrepancies with others [13,14,17,28].

At high incident energy (505 eV) [17], the energies for the $3s3p^6 4s(^3S)$ and $3s3p^6 4s(^1S)$ states were found to be 25.02 and 25.20 eV, supposing that the spin—orbit splitting is 0.180 eV. These values are in good agreement with other references cited in [17], and they were accepted as energies for these states. Comparison between the present low incident energy study and the high incident one [17] shows a difference of 35 meV for the $4s(^3S)$ and 90 meV for the $4s(^1S)$ state, probably due to the differences in energy resolution.

The spin-orbit splitting of the $4s(^{3,1}S)$ states obtained here is 0.305 eV. This value is different from the ones given in [12] (0.2 eV) and [14] (slightly below 0.2 eV), but in reasonably good agreement with the one of [26] (0.29 eV) and the tabulated value for the Mg atom from [29] (0.286 eV).

Another phenomenon that affects the observation of the $4s(^{3,1}S)$ states when approaching the excitation threshold is the PCI. This manifests in broadening and a shift of the peaks in the energy region between 32.74 and 27.68 eV.

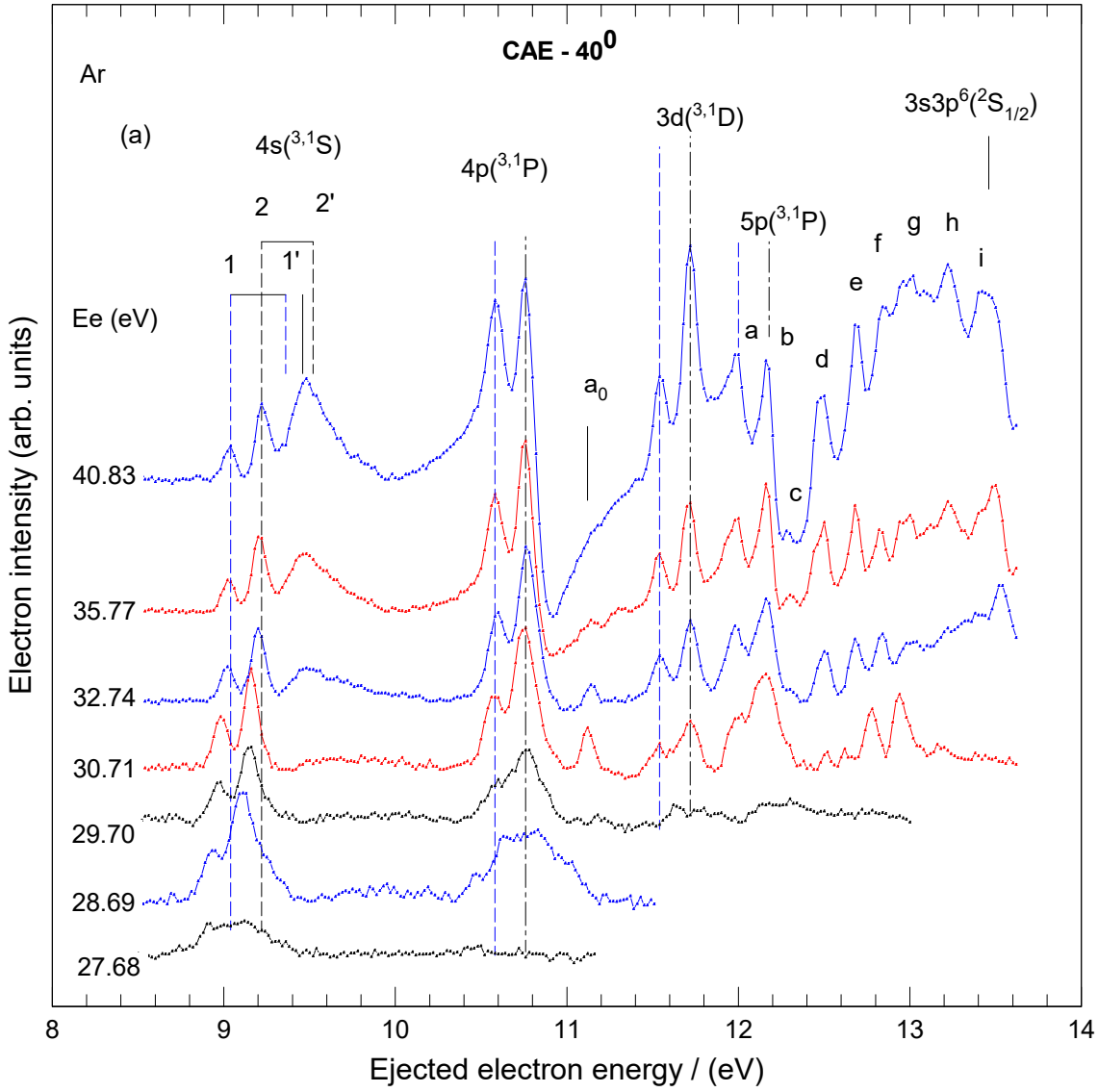

Figure 7. *Cont.*

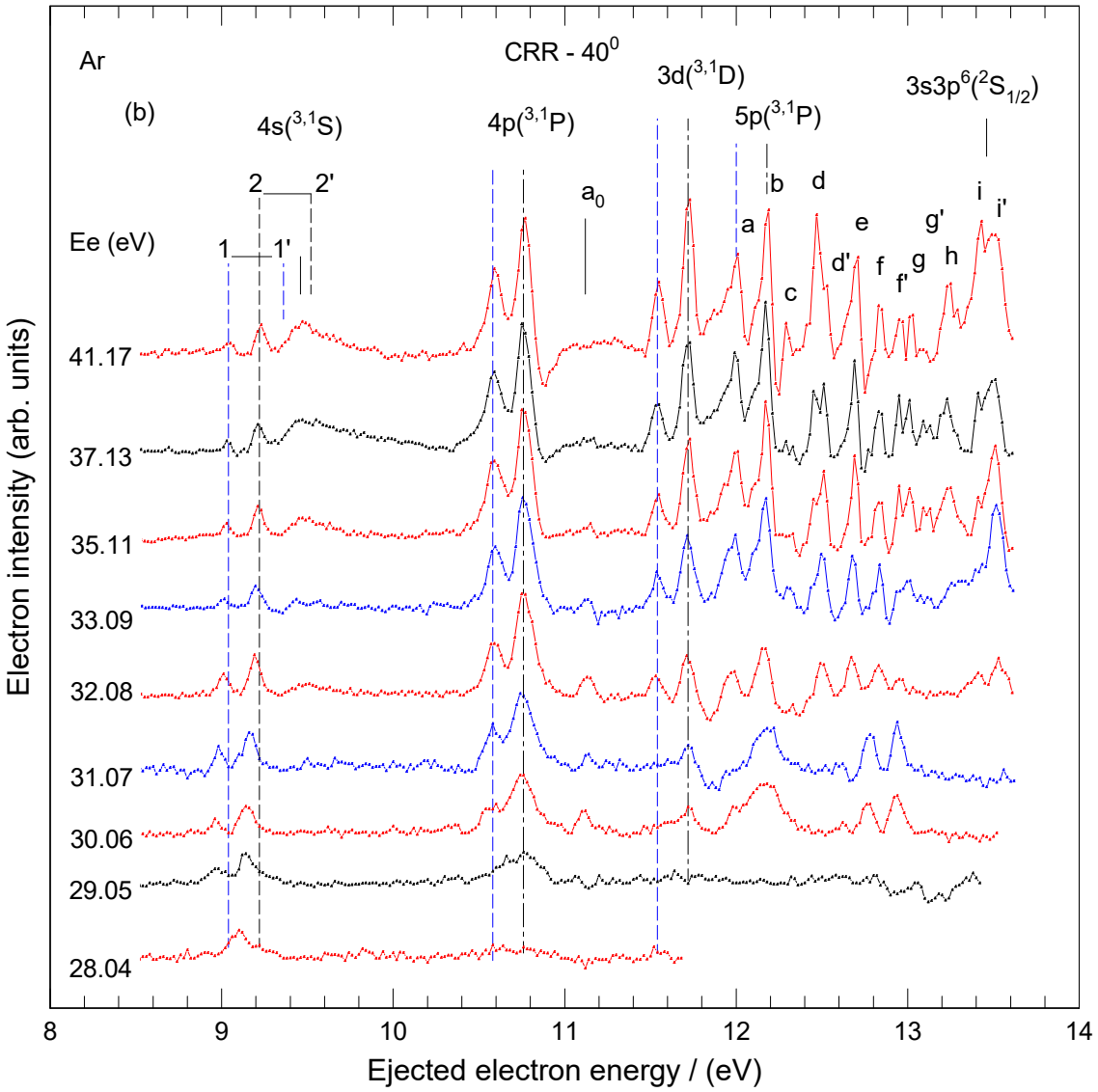

Figure 7. Series of background-subtracted ejected electron spectra at 40° in the kinetic energy region 8.5–13.6 eV: (**a**) The spectra obtained in the CAE mode at the incident energy between 27.68 and 40.83 eV; (**b**) The spectra obtained in the CRR mode at the incident energy region between 28.04 and 41.17 eV. The energy step was 0.020 eV. Incident electron energies are shown at the left-hand side. Long vertical dashed lines indicate the energies of the 4s(^{3,1}S), 4p(^{3,1}P), and 3d(^{3,1}D) excited states. Small Latin letters (a–i') indicate the energies of the single excited np (n ≥ 5) and nd (n ≥ 4) states listed in Table 1.

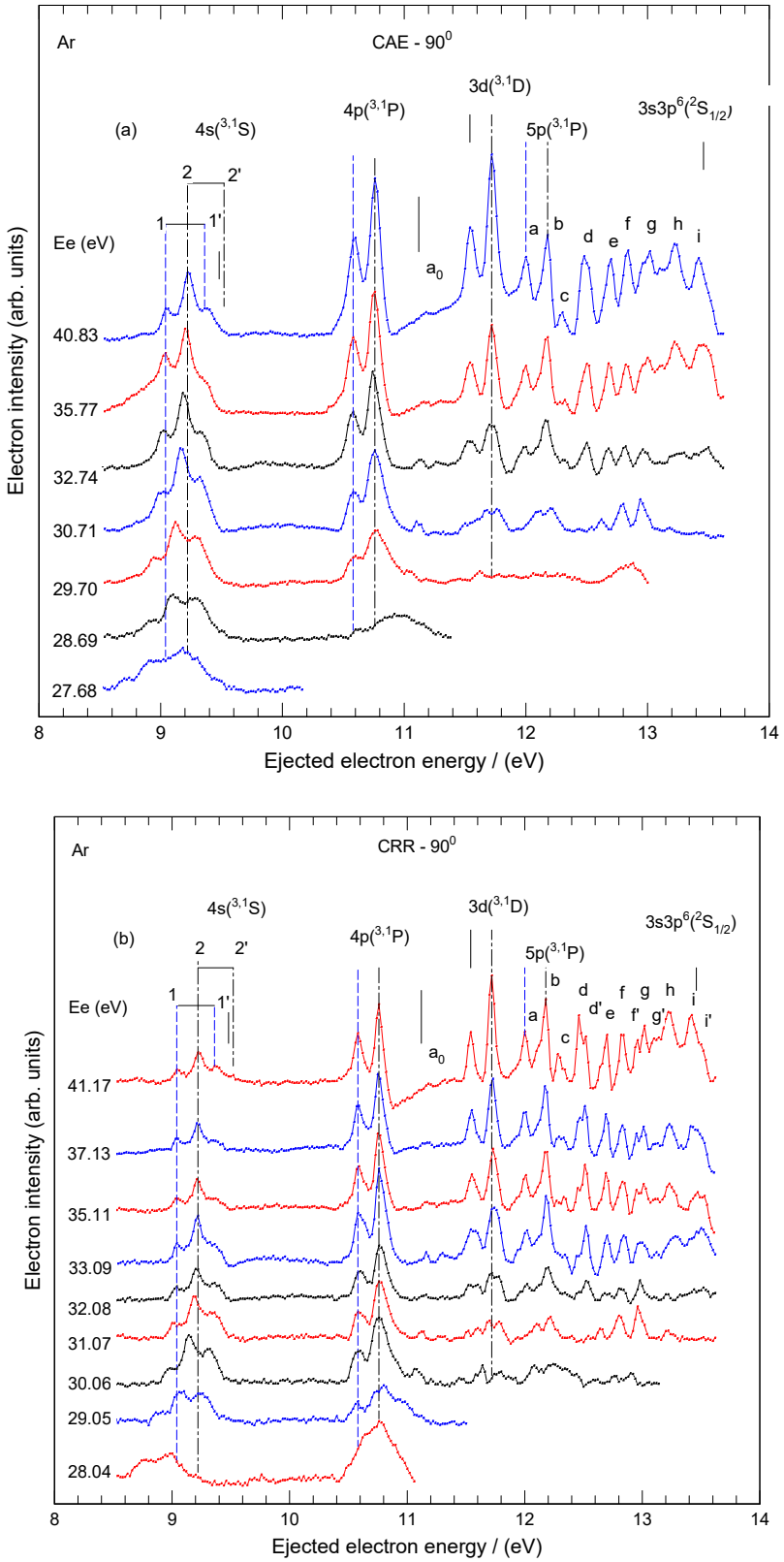

Figure 8. Series of background-subtracted ejected electron spectra at 90° in the kinetic energy region 8.5–13.6 eV: (**a**) The spectra obtained in the CAE mode at the incident energy between 27.68 and 40.83 eV; (**b**) The spectra obtained in the CRR mode at the incident energy region between 28.04 and 41.17 eV. The energy step was 0.020 eV. Incident electron energies are shown at the left-hand side. Long vertical dashed lines indicate the energies of the 4s(^{3,1}S), 4p(^{3,1}P), and 3d(^{3,1}D) excited states. Small Latin letters (a–i') indicate the energies of the single excited np ($n \geq 5$) and nd ($n \geq 4$) states listed in Table 1.

3.2.2. The 4p(^{3,1}P) States

These states clearly appear in all spectra as two not completely resolved peaks with a FWHM of 80 meV, always at the same energy position and with the energy separation of 0.18 eV. At high incident energy of 505 eV [17], the 4p(^{3,1}P) states showed up as two dips at kinetic energies 10.65 eV and 10.83 eV, which makes a difference of 70 meV from the kinetic energies of two peaks shown in Figure 10 at 10.58 eV and 10.76 eV. It should be noted that the second peak shows a Beutler–Fano resonant line shape. Taking into account that these two peaks have energy separation as the two terms of the ion core, we suppose that they are generated from the 4p(^{3}P) state at an energy of 26.52 eV (10.58 + 15.94), (10.76 + 15.76). Since the energy of the 4p(^{1}P) state obtained at high incident energy [17] is 26.59 eV, it follows that, within the ejected-electron detection method, the energies of the triplet and singlet 4p states can be determined only through a combination of experiments conducted at both high and low incident energies. Comparison with other references is shown in Table 1. For the 4p(^{3}P) state, very good agreement is found with [12–14]. For the 4p(^{1}P) state, a very good agreement is found with all references in the literature. In the energy-loss experiment reported in [12], the 4p(^{3}P) state was identified as an asymmetric peak at 26.56 eV with a natural width of 40 meV, while the position of the 4p(^{1}P) state was taken from optical measurement [18] at 26.606 eV. From the present and our previous [17] work, the spin-orbit splitting of the 4p states is (0.07 ± 0.02) eV (26.59–26.52). This value is far from 0.17 eV [10] and 0.16 eV [11].

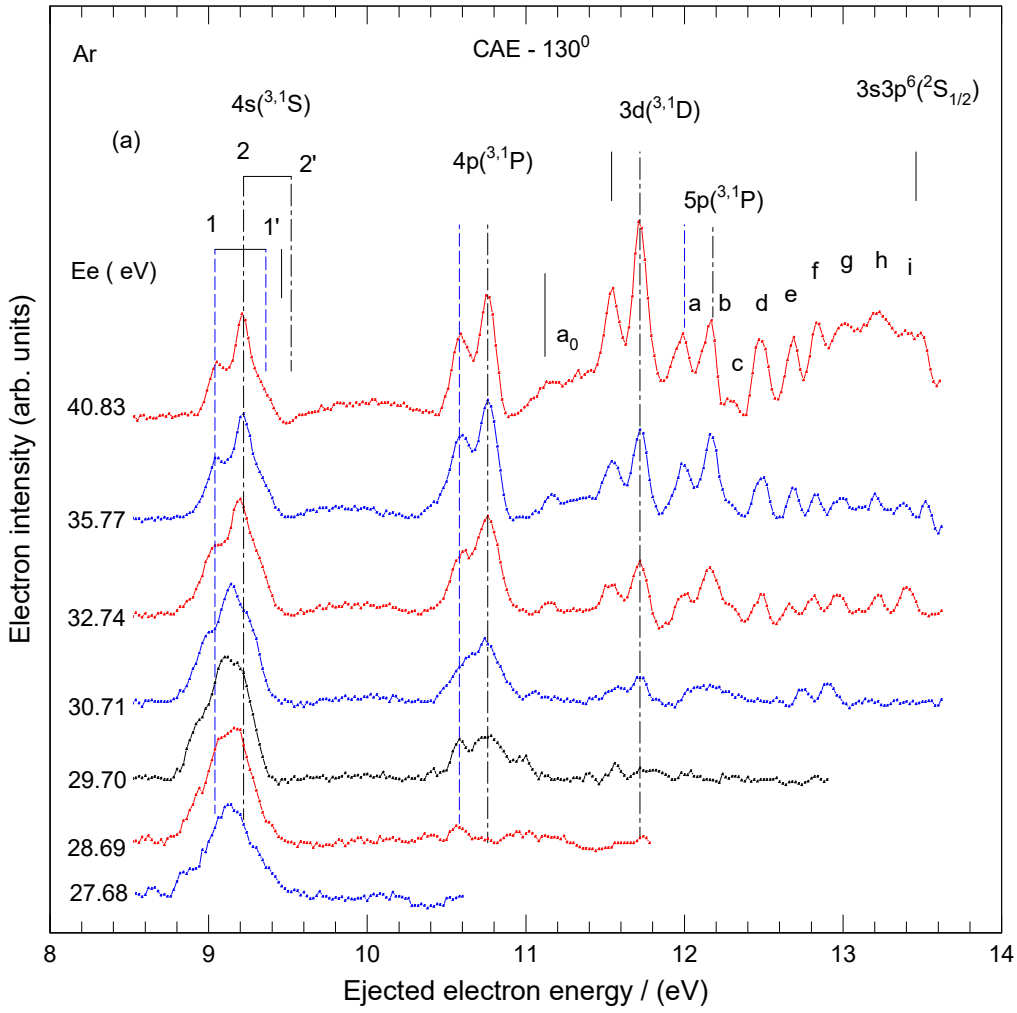

Figure 9. *Cont.*

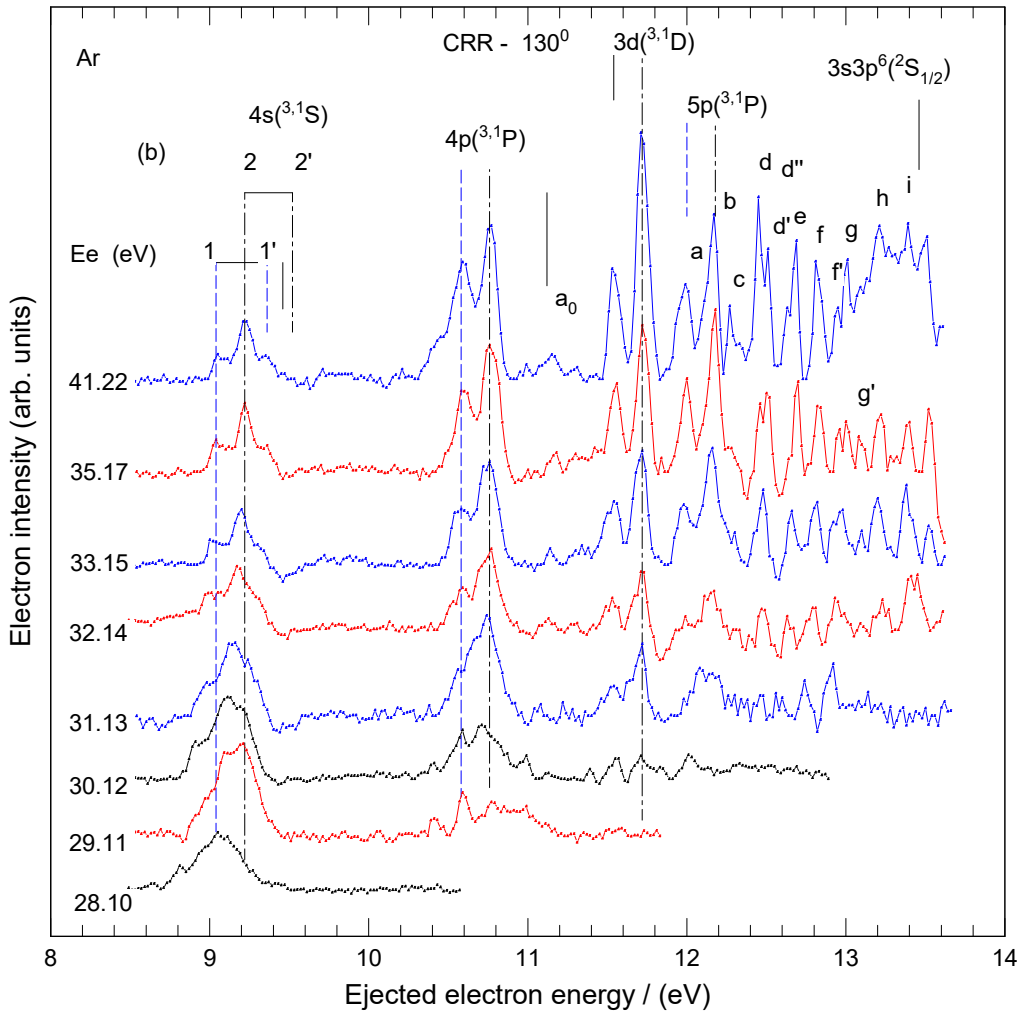

Figure 9. Series of background-subtracted ejected electron spectra at 130° in the kinetic energy region 8.5–13.6 eV: (**a**) The spectra obtained in the CAE mode at the incident energy between 27.68 and 40.83 eV; (**b**) The spectra obtained in the CRR mode at the incident energy region between 28.10 and 41.22 eV. The energy step was 0.020 eV. Incident electron energies are shown at the left-hand side. Long vertical dashed lines indicate the energies of the 4s(^{3,1}S), 4p(^{3,1}P), and 3d(^{3,1}D) excited states. Small Latin letters (a–i) indicate the energies of the single excited np ($n \geq 5$) and nd ($n \geq 4$) states listed in Table 1.

3.2.3. Doubly Excited $3s^2 3p^4(^3P, ^1D, ^1S)nln'l'$ States

The feature (a_0) at 11.12 eV kinetic energy or 26.88 eV excess energy appears in the spectra as a small peak with uncertain assignment. Its observation in a limited incident energy region (26.8–36.5 eV) between the 4p and 3d states from Figures 7–9 is predicted to be a manifestation of the doubly excited states with $3s^2 3p^4(^3P, ^1D, ^1S)nln'l'$ configurations [30]. The assignment to the $3s^2 3p^4(^3P)\ 4s^2(^3P)$ doubly excited state has been proposed by [28,30,31] for the structures at 26.82, 26.80, 26.85 eV, respectively. Thus, the assignment to the $3s^2 3p^4(^3P)\ 4s^2(^3P)$ doubly excited state is accepted for this feature.

3.2.4. The 3d(^{3,1}D) States

These states appear in all spectra as two peaks at kinetic energies 11.54 eV and 11.72 eV with an energy separation of 0.18 eV. These kinetic energies are the same at high [17] and low incident energies. Figures 7–9 show that this peak is observed in spectra with decreasing incident energies until 30 eV. The FWHM of this peak is between 60 and 70 meV, the best achieved resolution in the present work. In [17], the resolution achieved was 40 meV.

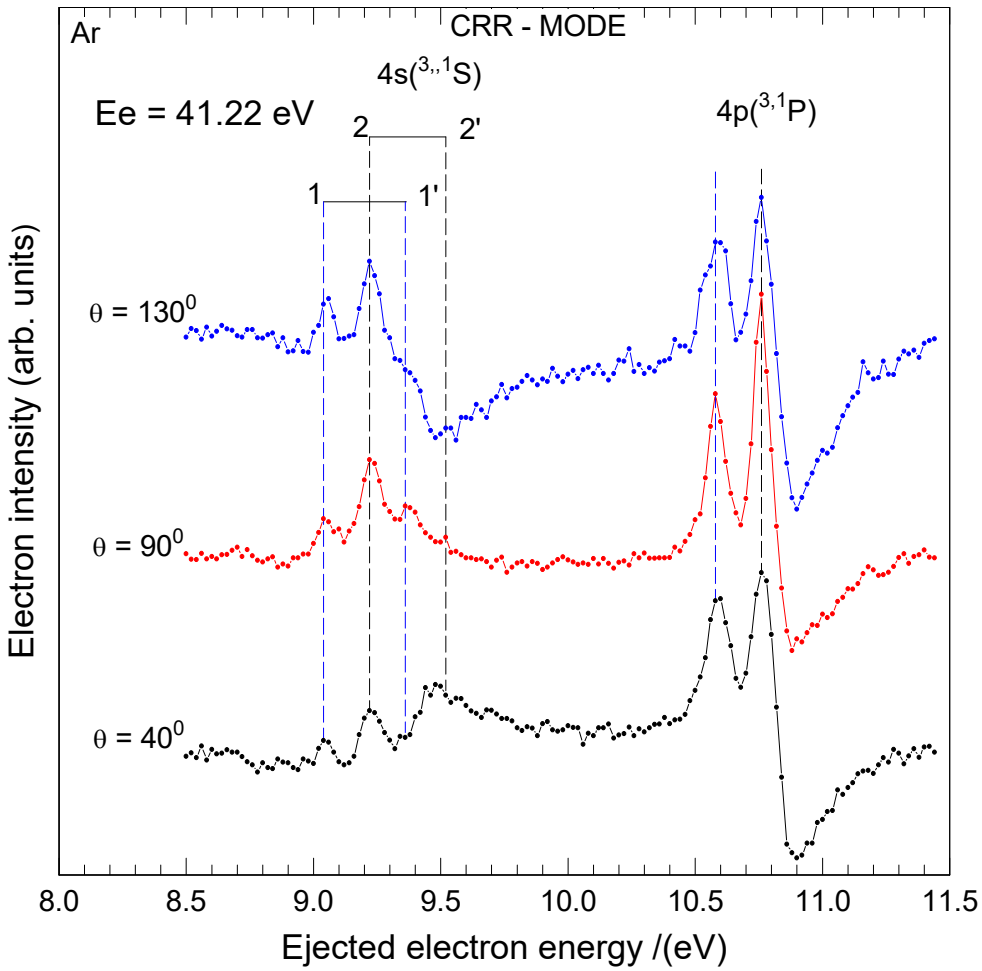

Figure 10. The ejected electron spectra at incident energy 41.22 eV were obtained in the CRR operation mode at ejected angles 40°, 90°, and 130°. All spectra are shown with the background subtracted. The energy step is 0.020 eV. The dashed long lines show the kinetic energies of the 4s and 4p peaks.

The excitation energy of the 3d states is the mean value of 27.48 eV (11.54 + 15.94) and 11.72 + 15.76) attributed only to the 3d(^{3}D) state at low incident energies and to the 3d(^{1}D) state at high incident energy [17]. Previous measurements give an energy of the 3d(^{1}D) state at 27.48 eV [11,32], 27.50 eV [13], and 27.51 eV [14,33] in good agreement with our value obtained at high energy. This means that the spin-orbit splitting of this state is small, not resolvable with the present experimental resolution. Similar conclusions have been reached in the energy-loss experiment [13] where the authors give two possible explanations: either the excitation probability for the ^{3}D state is smaller than that of the ^{1}D state or the splitting is very small (<15 meV). It should be noted that the absence of the 5s state. This state is expected to lie close to the 3d(^{1}D) state and may be unresolved due to insufficient spectral resolution or may exhibit a very low cross-section.

3.2.5. The 5p(^{3,1}P) States

The pair of features (a, b) at 12.00 and 12.18 eV with energy separation of 0.18 eV is identified as the 5p(^{3}P) state. At high incident energy [17], the 5p states appeared as two dips at kinetic energies 12.04 eV and 12.22 eV, which gives an equal energy difference of 40 meV between the experiments at high and low incident energies. As with the case of 4p states, the excitation energy of the 5p state is 27.94 eV (12.00 + 15.94), (12.18 + 15.76), and this value is attributed to the 5p(^{3}P) state. The comparison of the energy of the 5p(^{3}P) state with the only previous measurement [11] (27.93 eV) shows excellent agreement. The

excitation energy of the 5p(^{1}P) cannot be obtained from the spectra at low incident energies, and we accept its energy of 27.98 eV from the results at high incident energies [17]. This is in good agreement with the other measurement, i.e., 27.98 eV [17], 27.99 eV [11,25,34], and 28.00 eV [18,32,33,35]. The spin-orbit splitting of the 5p states is (40 ± 20) meV (27.98–27.94) eV. This value, with its uncertainty, is in good agreement with the calculated and experimental values of 58 and 60 meV [11], respectively. There are no other references for comparison. This procedure shows that energies and spin-orbit splitting of the excited states in ejected electron spectra can be obtained only by combining high and low incident energy experiments.

3.2.6. The 4d(^{3,1}D) States

The pair of features (c, d) at 12.30 and 12.48 eV with energy separation of 0.18 eV is identified as the 4d(^{3}D) state with a mean energy of 28.24 eV (12.30 + 15.94, 12.48 + 15.76). This energy is attributed to the 4d(^{3}D) state based on its appearance at low incident energies. The validity of this argument rests on the different energy dependences of the excitation cross sections for triplet and singlet states near threshold. The cross sections for triplet states exhibit an abrupt rise at threshold, followed by a rapid decrease with increasing energy. In contrast, the cross sections for singlet states increase monotonically, reaching a maximum at several times the excitation energy, and subsequently decrease according to the Bethe–Born $\ln(E_e)/E_e$ law. The existence of the 4d(^{1}D) state in the spectrum is uncertain; it may lie very close in energy but with a very small intensity. The spin-orbit splitting of these states is unknown, although it is expected to be smaller than that of the 3d states. On the other side, the energy 28.24 eV is attributed to the 4d(^{1}D) state in [17]. This is correct, but the energy of the 4d(^{3}D) state must be very close to this value. The comparison with other references in Table 1 shows good agreement between the energy of the 4d(^{1}D) state and the ones given by [11,13,32,33].

3.2.7. The 6p(^{3,1}P) States

The features (d′, e) at 12.52 and 12.70 eV with an energy separation of 0.18 eV are identified as the 3s3p^{6}6p(^{3,1}P) states. The mean energy of 28.46 eV is attributed to the 6p(^{3}P) state based on its appearances at low incident energies. This observation suggests that the 6p(^{1}P) state lies very close to the triplet state, with a very small spin—orbit splitting that is not resolvable with the present experimental resolution. Comparison with [17] shows that the energy 28.46 eV can be attributed to the 6p(^{1}P) state. Table 1 shows the excellent agreement between the energy of the 6p(^{1}P) state with [11,17] and very good agreement with other works [18,25,32–34], except with [35].

3.2.8. The 5d(^{3,1}D) States

The pair of features (d″, f) at 12.64 and 12.82 eV with energy separation 0.18 eV does not appear in all spectra. The feature (d″) appears as a shoulder in Figure 3b, while the feature (f) is present in all spectra as a peak. The features are identified as the 3s3p^{6}5d(^{3,1}D) states. The mean energy of 28.58 eV is attributed to the 5d(^{3}D) state due to its appearance at low incident energy, while the 5d(^{1}D) state should lie close to the triplet state, but the spin—orbit splitting is unknown. Comparison with [17] shows that the energy of 28.58 eV of the 5d(^{1}D) state is correct. In the absence of numerical data for the 5d(^{3}D) state, a comparison with literature is possible only for the 5d(^{1}D) state. An excellent agreement is found with references [11,17], good agreement with references [4,33], and some discrepancy with other works [25,32,35].

3.2.9. Higher n States

Identification of all other small peaks from Figures 7–9 below the ionization potential of the 3s state is uncertain due to the overlapping of a large number of states. However, if we suppose that the states decay directly to the triplet term of the ion core, then their energies shown in Table 1 represent triplet components of the corresponding states.

Finally, in the comparison of results between lower and higher incident energies [17], one can notice the absence of the cusp-like feature in all figures at 13.48 (29.24) eV, the ionization potential of the 3s subshell. The reason for this is the large number of excited states approaching the ionization potential. The comparison between the CAE and CRR modes shows that the CRR mode has a better resolution and lower contribution of the scattered electrons, as witnessed by the shape of the spectra above the 4s(^{1}S) state region.

Table 1. Kinetic energy, KE(eV), and excitation energies (eV) of Ar autoionizingstates obtained from excitation of the 3s electron to 3s3p^6 (ns, np, nd) states in the ejected energy region from 9 to 14 eV (24.76 to 29.76 eV of excitation energies) at incident electron energies 27–41 eV and three ejection angles 40°, 90° and 130°. References: Brion and Olsen [4], Veillette and Marchand [10], Fryar and McConkey [11], Wilden et al. [12], Mitchell et al. [13], Roy et al. [14], Jureta et al. [17], Madden et al. [18], Tweed et al. [25], Bolduc et al. [26], Simpson et al. [27], NIST [29], Lefaivre et al. [30], Veillette et al. [31], Marchand and Cardinal. [28], Bergmark et al. [33], McConkey and Preston [32], Peresse et al. [35], Wu et al. [34].

This Work		Reference	Exc. En. (eV)	Assignment
Label	**KE (eV)**			
1–2	9.05 9.22	This work, Ee = 41 eV [10–14,17,26,28]	24.985 25.02, 25.02, 25.03, 25.03, 25.03, 25.02,24.96, 24.95	3s3p^{6}4s(^{3}S)
1′–2′	9.36 9.52	This work, Ee = 41 eV [4,10–14,17,26–28,33]	25.29 25.22, 25.26, 25.27, 25.23, 25.20, 25.21, 25.20, 25.25, 25.25, 25.20, 25.22	3s3p^{6}4s(^{1}S)
	10.58 10.76	This work, Ee = 41 eV [10–14,17,28]	26.52 26.41, 26.46, 26.56, 26.55, 26.59, 26.41, 26.35	3s3p^{6}4p(^{3}P)
	/	[10,11,13,14,17,18,25,26,28,32,33]	26.58, 26.62, 26.61, 26.62, 26.59, 26.606, 26.60, 26.60, 26.65, 26.62, 26.63	3s3p^{6}4p(^{1}P)
(a_0):	11.12	This work [28,30,31]	26.88 26.82, 26.80, 26.85	3s^{2}3p^4(^{3}P) 4s^2(^{3}P)
	11.54 11.72	This work [10,26,28]	27.48 27.42, 27.43, 27.45	3s3p^{6}3d(^{3}D)
	/	[10,11,13,14,17,25,26,28,32,33]	27.63, 27.48, 27.50, 27.51, 27.48, 27.54, 27.61, 27.65, 27.51, 27.48	3s3p^{6}3d(^{1}D)
(a) (b)	12.00 12.18	This work [11]	27.94 27.93	3s3p^{6}5p(^{3}P)
	/	[11,17,18,25,32–35]	27.99, 27.98, 27.996, 27.99, 27.997, 28.02, 28.00, 27.994	3s3p^{6}5p(^{1}P)
(c) (d)	12.30 12.48	This work	28.24	3s3p^{6}4d(^{3}D)
	/	[4,11,13,17,25,32–35]	28.30, 28.24, 28.27, 28.24, 28.35, 28.27, 28.29, 28.35, 28.33	3s3p^{6}4d(^{1}D)

Table 1. *Cont.*

This Work Label	This Work KE (eV)	Reference	Exc. En. (eV)	Assignment
(d′) (e)	12.52 12.70	This work	28.46	$3s3p^6 6p(^3P)$
	/	[11,17,18,25,32–35]	28.49, 28.49, 28.509, 28.51, 28.51, 28.50, 28.55, 28.509	$3s3p^6 6p(^1P)$
(d″) (f)	12.64 12.82	This work	28.58	$3s3p^6 5d(^3D)$
	/	[4,11,17,25,32,33,35]	28.64, 28.59, 28.58, 28.70, 28.62, 28.70, 28.70	$3s3p^6 5d(^1D)$
(f′)	12.96	This work [11,18,33]	28.72 28.71, 28.75, 28.75	$3s3p^6 7p(^{3,1}P)$
(g)	13.01	This work [4,11], (calc.)	28.77 28.83, 28.79	$3s3p^6 6d(^{3,1}D)$
(g′)	13.10	This work [11,18,33], (calc.)	28.86 28.86, 28.89, 28.89	$3s3p^6 8p(^{3,1}P)$
(h)	13.23	This work [4,11], (calc.)	28.99 29.01, 28.99	$3s3p^6 7d(^{3,1}D)$
(i)	13.42	This work	29.18	
	13.46	[29,32], I.P.(3s)	29.24, 29.22	$Ar^+ 3s3p^6(^2S_{1/2})$

4. Conclusions

In this work, we have studied the auto-ionizing states in helium and argon at low incident energy region. We mainly concentrate on triplet states, which are preferentially excited at low energies and larger scattering angles. We exploit a high-resolution electron spectrometer and two modes of operation, CAE and CRR, to obtain the spectra of the ejected electrons. We studied spin-orbit splitting as well as the doublet structure of peaks due to the existence of two close ion core states on which auto-ionizing states decay. We also studied the PCI effect on the $(2s^2)^1S$ state of helium, and we concluded that the behavior of shift versus excess energy is in full agreement with the previous measurements [7,9].

Energies of the $4s(^3S)$ and $4p(^3P)$ states of argon are found to be 24.985 and 26.52 eV, respectively. The spin-orbit splitting of 0.305 eV is found for the 4s states and 0.07 eV for the 4p states. Further studies of higher series of auto-ionizing states would need the improvement of signal–to–noise ratio and a mode of operation which distinguishes between scattered and ejected electrons.

One of the principal conclusions drawn from the present study at low incident energies, together with our earlier investigations at higher incident energies, is that accurate determination of auto-ionization-state energies requires measurements at both low- and high-energy regimes. As noted above, this necessity arises from the different energy dependences of the excitation cross sections for triplet and singlet states, and ultimately from the presence of post-collision interaction (PCI) effects. A similar conclusion was also reported previously in [7].

Author Contributions: Conceptualization, J.J.J. and B.P.M.; methodology, J.J.J.; software, J.J.J. and B.P.M.; validation, J.J.J., B.P.M. and L.A.; formal analysis, J.J.J., B.P.M. and L.A.; investigation, J.J.J.; resources, J.J.J. and B.P.M.; data curation, J.J.J. and B.P.M.; writing—original draft preparation, J.J.J.; writing—review and editing, J.J.J., B.P.M. and L.A.; visualization, J.J.J., B.P.M. and L.A.; supervision,

B.P.M. and L.A.; project administration, B.P.M. and L.A.; funding acquisition, B.P.M. and L.A. All authors have read and agreed to the published version of the manuscript.

Funding: This research was funded by the Science Fund of the Republic of Serbia, grant number 6821, Project title "Atoms and (bio)molecules-dynamics and collisional processes on short time scale" (ATMOLCOL).

Data Availability Statement: Data are contained within the article.

Acknowledgments: The work has been performed within the Italy and Serbia bilateral project of particular relevance (Grande Rilevanza) "Nanoscale insights in radiation damage". One of us, J.J.J., is grateful to the Institute of Physics Belgrade for being allowed to use their material resources.

Conflicts of Interest: The authors declare no conflicts of interest.

Abbreviations

The following abbreviations are used in this manuscript:

CEA	Constant Analyzer Energy
CRR	Constant Retarding Ratio
PCI	Post-Collision Interaction
FWHM	Full Width at Half Maximum

References

1. de Harak, B.A.; Childers, J.G.; Martin, N.L.S. Ejected electron spectrum of He below the N = 2 threshold. *Phys. Rev. A* **2006**, *74*, 032714. [CrossRef]
2. Avaldi, L.; Jureta, J.J.; Marinković, B.P. Energy analysis of ejected electrons in the region of the Ar L_1-$L_{2,3}$M Coster-Kronig transitions (25–56 eV) induced by electron impact. *J. Electron Spectrosc. Rel. Phenom.* **2019**, *237*, 146898. [CrossRef]
3. Comer, J.; Read, F.H. Electron impact studies of autoionizing states in neon and helium. *J. Electron Spectrosc. Rel. Phenom.* **1972**, *1*, 3–11. [CrossRef]
4. Brion, C.E.; Olsen, L.A.R. Threshold electron impact excitation of the rare gases. *J. Phys. B Atom. Mol. Phys.* **1970**, *3*, 1020–1033. [CrossRef]
5. Oda, N.; Nishimura, F.; Tachira, S. Energy spectra of electrons from autoionization states in helium by electron impact. *Phys. Rev. Lett.* **1970**, *24*, 42–45. [CrossRef]
6. Hicks, P.J.; Cvejanović, S.; Comer, J.; Read, F.H.; Sharp, J.M. Displacements of electron ejection energies in near- threshold excitation of autoionizing levels of helium by electron impact. *Vacuum* **1974**, *24*, 573–580. [CrossRef]
7. Smith, A.J.; Hicks, P.J.; Read, F.H.; Cvejanovic, S.; King, G.C.M.; Comer, J.; Sharp, J.M. Phenomena associated with near-threshold excitation of autoionizing levels of helium by electron impact. *J. Phys. B Atom. Mol. Phys.* **1974**, *7*, L496–L502. [CrossRef]
8. Hicks, P.J.; Comer, J. Ejected electron spectroscopy of autoionizing states excited by low energy electron impact. *J. Phys. B Atom. Mol. Phys.* **1975**, *8*, 1866–1879. [CrossRef]
9. Spence, D. Cross sections and threshold effects for electron-impact excitation of the $(2s^2)^1S$ and $(2s2p)^3P$ states of helium. *Phys. Rev. A* **1975**, *12*, 2353–2359. [CrossRef]
10. Veillette, P.; Marchand, P. Excitation par impact électronique des états $3s3p^6nl$ de l'argon. *Can. J. Phys.* **1974**, *52*, 930–934. [CrossRef]
11. Fryar, J.; McConkey, J.W. Analysis of the ejected-electron spectra of Ar following controlled electron impact. *J. Phys. B Atom. Mol. Phys.* **1976**, *9*, 619–629. [CrossRef]
12. Wilden, D.G.; Comer, J.; Hicks, P.J. Threshold effects in the excitation of autoionising states of argon atom by electron impact. *Nature* **1978**, *273*, 651–653. [CrossRef]
13. Mitchell, P.; Baxter, J.A.; Comer, J.; Hicks, P. The excitation of autoionising states of argon by electron impact. *J. Phys. B Atom. Mol. Phys.* **1980**, *13*, 4481–4494. [CrossRef]
14. Roy, D.; Poulin, A.; Hubin-Franskin, M.J.; Delwiche, J. Electron scattering and electron ejection by argon in the range 24–29 eV. *J. Electron Spectros. Relat. Phenom.* **1980**, *19*, 101–114. [CrossRef]
15. Bartschat, K.; Bray, I.; Fursa, D.V. Benchmark Calculations for Near-Threshold Electron-Impact Excitation of the $(1s3s)^{3,1}S$ States of Helium. *Atoms* **2025**, *13*, 27. [CrossRef]
16. Jureta, J.J.; Milosavljević, A.R.; Marinković, B.P. High energy electron impact study on autoionizing region in helium by detection of ejected electrons. *Int. J. Mass. Spectrom.* **2014**, *365–366*, 114–120. [CrossRef]

17. Jureta, J.J.; Marinković, B.P.; Avaldi, L. Energy and angular analysis of ejected electrons (6–26 eV) from the autoionization regions of argon at incident electron energies 505 and 2018 eV. *Eur. Phys. J. D* **2016**, *70*, 199. [CrossRef]
18. Madden, R.P.; Ederer, D.L.; Codling, K. Resonances in the Photo-ionization Continuum of Ar I (20–150 eV). *Phys. Rev.* **1969**, *177*, 136–151. [CrossRef]
19. Madden, R.P.; Codling, K. New autoionizing atomic energy levels in He, Ne, and Ar. *Phys. Rev. Lett.* **1963**, *10*, 516–518. [CrossRef]
20. van den Brink, J.P.; van Eck, J.; Heideman, H.G. Interference between scattered and ejected electrons in e-He collisions: A new probe for coherence studies. *Phys. Rev. Lett.* **1988**, *61*, 2106–2108. [CrossRef]
21. van der Burgt, P.J.M.; van Eck, J.; Heideman, H.G.M. Orbital Angular Momentum Exchange in Post-Collision Interaction. In *Fundamental Processes in Atomic Collision Physics*; Kleinpoppen, H., Briggs, J.S., Lutz, H.O., Eds.; NATO ASI Series; Springer: Boston, MA, USA, 1985; Volume 134, pp. 619–625. [CrossRef]
22. van der Burgt, P.J.M.; van Eck, J.; Heideman, H.G.M. Orbital angular momentum exchange in post-collision interaction. *J. Phys. B Atom. Mol. Phys.* **1985**, *18*, 999–1009. [CrossRef]
23. Jureta, J.J.; Marinković, B.P.; Avaldi, L. The $N_{4,5}$-OO Auger and "N_3"-$M_{4,5}O_{2,3}$ Coster-Kronig spectra of xenon induced by electron impact. *Adv. Space Res.* **2023**, *71*, 1338–1351. [CrossRef]
24. van den Brink, J.P.; den Outer, P.N.; van Eck, J.; Eideman, H.G.M. Coherence and correlation in electron impact autoionisation of neon and argon. *J. Phys. B At. Mol. Opt. Phys.* **1990**, *23*, 2349–2362. [CrossRef]
25. Tweed, R.J.; Gelebart, F.; Peresse, J. Autoionization by electron impact: Experiments on Ar, Kr and Xe. *J. Phys. B Atom. Mol. Phys.* **1976**, *9*, 2643–2656. [CrossRef]
26. Bolduc, E.; Quéméner, J.J.; Marmet, P. Electron-Impact Excitation of $3s3p^6nl$ States of Ar. *Can. J. Phys.* **1971**, *49*, 3095–3098. [CrossRef]
27. Simpson, J.A.; Chamberlain, G.E.; Mielczarek, S.R. Excitation of Optically Forbidden States in the Ionization Continuum by Electron Impact. *Phys. Rev.* **1965**, *139*, A1039–A1041. [CrossRef]
28. Marchand, P.; Cardinal, J. Metastable yield of argon between 23 and 37 eV by electron impact. *Can. J. Phys.* **1979**, *57*, 1624–1633. [CrossRef]
29. Kramida, A.; Ralchenko, Y.; Reader, J.; NIST ASD Team. *NIST Atomic Spectra Database (Ver. 5.12)*; National Institute of Standards and Technology: Gaithersburg, MD, USA, 2024. Available online: https://physics.nist.gov/asd (accessed on 16 December 2025). [CrossRef]
30. Lefaivre, D.; Marmet, P. Electron excitation of Ar between 26 and 34 eV. *Int. J. Mass Spectrom. Ion Phys.* **1975**, *18*, 153–164. [CrossRef]
31. Veillette, P.; Marchand, P. Photon detection of doubly excited states of argon produced by electron impact. *Int. J. Mass Spectrom. Ion Phys.* **1975**, *18*, 165–178. [CrossRef]
32. McConkey, J.W.; Preston, J.A. Autoionizing states in argon. *J. Phys. B Atom. Mol. Phys.* **1973**, *6*, L138–L141. [CrossRef]
33. Bergmark, T.; Spohr, R.; Magnusson, N.; Werme, L.O.; Nordhng, C.; Siegbahn, K. *Uppsala University Institute of Physics Report No. 589*; Uppsala University Institute of Physics: Uppsala, Sweden, 1969.
34. Wu, S.L.; Zhong, Z.P.; Feng, R.F.; Xing, S.L.; Yang, B.X.; Xu, K.Z. Electron-impact study in valence and autoionization resonance regions of argon. *Phys. Rev. A* **1995**, *51*, 4494–4500. [CrossRef] [PubMed]
35. Peresse, J.; Gelebart, F.; Le Nadan, A. Autoionisation de l'argon par impacts d'électrons lents. *C. R. Acad. Sci. Ser. B* **1972**, *275*, 255–257.